Journal of Atmospheric and Solar-Terrestrial Physics xxx (xxxx) 106305

Contents lists available at ScienceDirect

Journal of Atmospheric and Solar-Terrestrial Physics

journal homepage: www.elsevier.com/locate/jastp

Research Paper

The Forbush decrease observed by the SEVAN particle detector network in the 25th solar activity cycle

T. Karapetyan[a,*], A. Chilingarian[a], G. Hovsepyan[a], H. Martoyan[a], B. Sargsyan[a], R. Langer[b], J. Chum[c], N. Nikolova[d], Hristo Angelov[e], Diana Haas[f], Johannes Knapp[g], Michael Walter[g], Ondrej Ploc[h], Jakub Šlegl[h], Martin Kákona[h], Iva Ambrožová[h]

[a] *A. I. Alikhanyan National Laboratory (Yerevan Physics Institute), Armenia*
[b] *Institute of Experimental Physics SAS, Košice, Slovakia*
[c] *Institute of Atmospheric Physics of the Czech Academy of Sciences, Prague, Czech Republic*
[d] *Basic Environmental Observatory Moussala Lab (Institute for Nuclear Research and Nuclear Energy, Bulgarian Academy of Sciences), Bulgaria*
[e] *Basic Environmental Observatory Moussala Lab (Institute for Nuclear Research and Nuclear Energy, Bulgarian Academy of Sciences), Bulgaria*
[f] *Deutsches Elektronen-Synchrotron DESY, Hamburg, Germany*
[g] *Deutsches Elektronen-Synchrotron DESY, Zeuthen, Germany*
[h] *Nuclear Physics Institute of the CAS, v.v.i., Rez, Czech Republic*

ARTICLE INFO

Handling editor: Dora Pancheva

Keywords:
Forbush decrease
ICME
Barometric coefficient
Geomagnetic field
Atmospheric electric field

ABSTRACT

The temporal variations of cosmic-ray intensity, measured by ground-based detectors at various latitudes, longitudes, and altitudes, are related to the geophysical and solar phenomena. The latter are interplanetary coronal mass ejections and fast solar wind from coronal holes, which cause interplanetary magnetic field (IMF) abrupt variations near Earth. Interacting with the magnetosphere, they cause worldwide sudden decreases (Forbush decreases, FDs) of intensity followed by gradual recovery. The amplitude of the flux depletion depends on the type and energy of the registered particle, which in turn depends on geographical coordinates and the detector's energy threshold and selective power. SEVAN particle detector network with nodes in Europe and Armenia selects three types of particles that demonstrate coherent depletion and recovery and correspond to different energy galactic protons interacting with disturbed magnetospheric plasmas.

On November 3–4, 2021, an interplanetary coronal mass injection (ICME) hit the magnetosphere, sparking a strong G3-class geomagnetic storm and auroras as far south as California and New Mexico. All detectors of the SEVAN network have registered an (FD) of ≈5% depletion in a 1-min time series of count rates. Approaching the maximum solar activity cycle, large variations of the particle flux intensity were registered on February 27, March 23, 2023, and March 24, 2024.

In this work, we present measurements of these FDs performed on mountain altitudes on Aragats (Armenia), Lomnicky Stit (Slovakia), Mileshovka (Czechia), and at sea level DESY (Hamburg, Germany). We compared FD measurements made by SEVAN detectors and neutron monitors located on Aragats and Lomnicky Stit and made a correlation analysis of FD registration at different locations.

1. Introduction

The Sun is a tremendously variable object, capable of modulating galactic cosmic ray (GCR) fluxes and sending intense solar cosmic rays (SCR) fluxes in the Earth's direction. The Sun "modulates" the low-energy GCRs in several ways. Along with broad-band electromagnetic radiation, the explosive flaring processes on the Sun usually result in Coronal Mass Ejections (CMEs) and acceleration of copious electrons and ions. Immense magnetized plasma structures, usually headed by shock waves, travel into the interplanetary space with velocities up to 3000 km/s (so-called interplanetary coronal mass ejection – ICME) and disturb the interplanetary magnetic field (IMF) and magnetosphere. These disturbances can lead to major geomagnetic storms harming multi-billion assets in space and on the ground. At the same time, these

* Corresponding author.
E-mail addresses: ktigran79@gmail.com (T. Karapetyan), chili@aragats.am (A. Chilingarian), nikol@inrne.bas.bg (N. Nikolova), hangelov@inrne.bas.bg (H. Angelov).

https://doi.org/10.1016/j.jastp.2024.106305
Received 30 January 2024; Received in revised form 10 June 2024; Accepted 10 July 2024
1364-6826/© 20XX

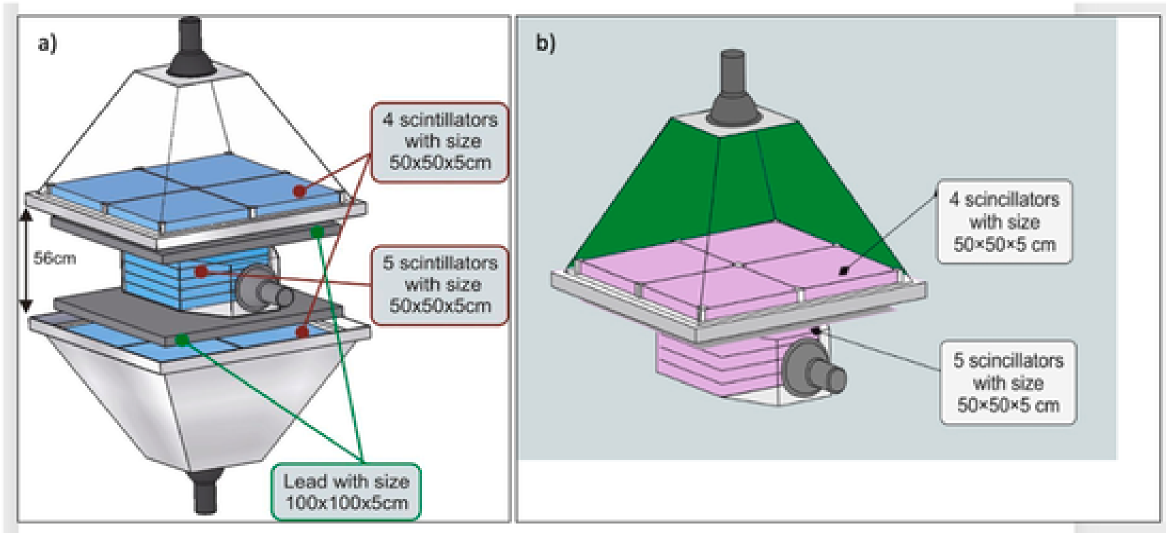

Fig. 1. Basic SEVAN detector(1a) and SEVAN-light detector (1b).

Table 1
Purity of the SEVAN coincidences measuring the ambient population of secondary cosmic ray flux (background) on Aragats (3200 m) in percent.

Coincidence	neutron	proton	mu +	mu-	e^-	e^+	γ
001	12.75	1.29	43.52	37.65	1.13	1.20	2.50
111	0.78	1.45	51.47	44.28	0.42	1.50	0.12
110	8.70	5.40	34.30	30.55	7.46	10.24	3.36
100	6.74	3.76	27.74	24.36	11.69	9.68	16.03
011	9.27	0.59	47.38	41.00	0.09	0.31	1.36
101	0.53	1.51	52.18	45.56	0.07	0.12	0.04
010	52.05	0.33	8.41	7.86	1.60	1.65	28.09

disturbances introduce anisotropy in the GCR flux. Thus, the time series of intensities of high-energy particles can provide highly cost-effective information also for the forecasting of geomagnetic storms (Leerungnavarat et al., 2003).

The networks of particle detectors located at different geographical coordinates and measuring various species of secondary cosmic rays are vital for basic research on solar physics, solar-terrestrial connections, and space weather, as well as for establishing alerting and forecasting services for dangerous consequences of space storms (Gevorgyan et al,. 2005).

In 1957, in unprecedented international cooperation, more than 66.000 scientists and engineers from 67 nations measured the major geophysical parameters in the framework of the International Geophysical Year (IGY1957; Chapman, 1959).

Fifty years on, the International Heliophysical Year (IHY 2007, Thompson et al., 2009) again drew scientists and engineers from around the globe in a coordinated observation campaign of the heliosphere and its effects on planet Earth. The United Nations Office for Outer Space Affairs, through the United Nations Basic Space Science Initiative (UNBSSI), assisted scientists and engineers worldwide in participating in the IHY. One of the most successful projects of IHY 2007was deploying arrays of small, inexpensive instruments worldwide to get global measurements of ionospheric and heliospheric phenomena. The small instrument program was (and still is) a partnership between instrument developers and instrument hosts in developing countries. The lead scientist prepared and installed the instruments and helped to run them; the host countries provided manpower for instrument operation and maintenance. The lead scientist's institution developed joint databases and prepared tools for user-friendly access to the data. It assisted in staff training and paper writing to promote space science activities in developing countries.

A network of particle detectors located at middle to low latitudes, known as SEVAN (Space Environment Viewing and Analysis Network, Fig. 1, Chilingarian et al., 2009, 2018), was developed in the framework of the International Heliophysical Year (IHY-2007) and now operates and continues to expand within International Space Weather Initiative (ISWI). SEVAN detectors measure time series of charged and neu-

Table 2
Barometric coefficients, count rates, and relative errors calculated for the SEVAN detector (October 26–28 data, 2018, 19 mb total change in the atmospheric pressure).

Detector	Alt. (m.)	Rc (GV)	Barometric Coeff. %/mb (Oct-2018)	Correlation Coefficient	1 min count rate [mean]	Relative Error	$\frac{1}{\sqrt{N}}$
SEVAN Aragats Upper 5 cm	3200	7.1	−0.33 ± 0.02	−0.986	29333	0.006	0.006
SEVAN Aragats Middle 20 cm	3200	7.1	−0.32 ± 0.02	−0.984	7848	0.011	0.011
SEVAN Aragats Lower 5 cm	3200	7.1	−0.25 ± 0.01	−0.981	17652	0.008	0.008
SEVAN Aragats Coincidence 100 (low energy charged particles)	3200	7.1	−0.38 ± 0.02	−0.984	20246	0.007	0.007
SEVAN Aragats Coincidence 010 (mostly neutrons and gamma rays)	3200	7.1	−0.47 ± 0.04	−0.966	2297	0.020	0.020
SEVAN Aragats Coincidence 111 (high energy muons)	3200	7.1	−0.19 ± 0.001	−0.966	3465	0.020	0.020
SEVAN Aragats Coincidence 101&111 (high energy muons)	3200	7.1	−0.19 ± 0.001	−0.966	7754	0.010	0.010
SEVAN Aragats Coincidence 101	3200	7.1	−0.19 ± 0.001	−0.949	4289	0.015	0.015
SEVAN Aragats Coincidence 110	3200	7.1	−0.41 ± 0.03	−0.963	1333	0.030	0.030
SEVAN Aragats Coincidence 011	3200	7.1	−0.27 ± 0.01	−0.929	753	0.040	0.040
SEVAN Aragats Coincidence 001	3200	7.1	−0.30 ± 0.02	−0.977	9144	0.010	0.010

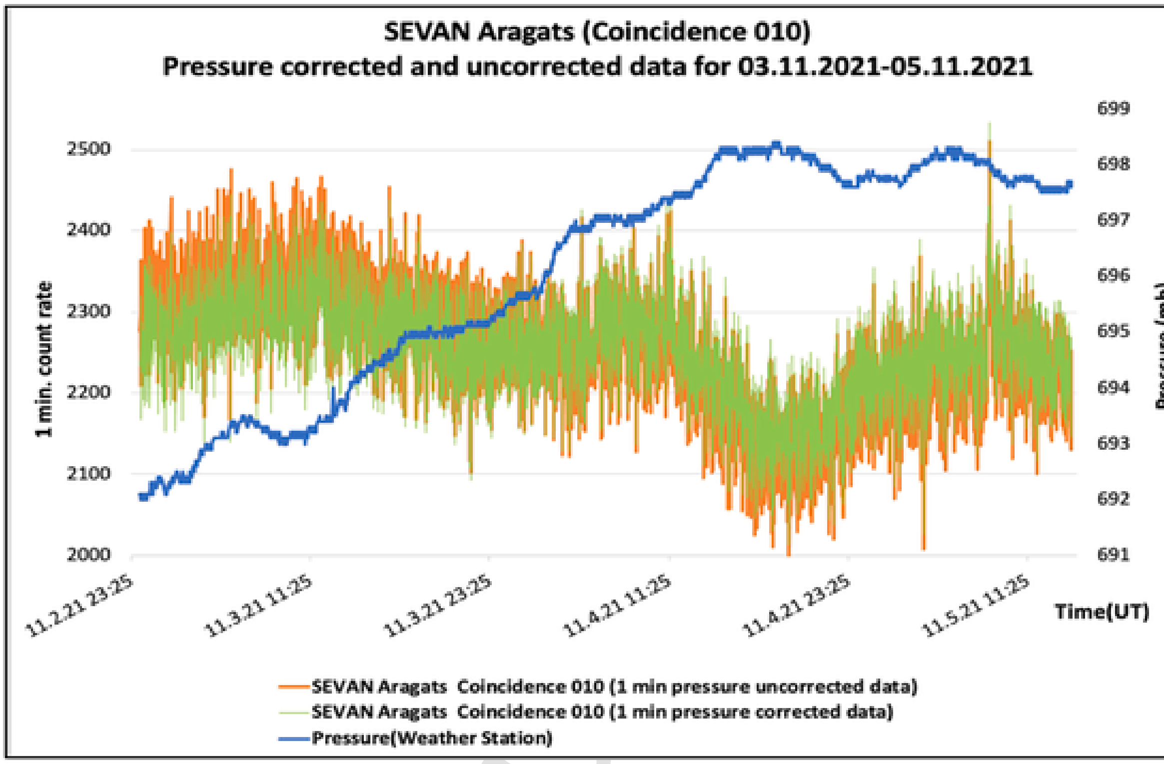

Fig. 2. One-minute time series of pressure corrected and uncorrected count rates of SEVAN “010” (neutral particles) counts. By the blue curve, the atmospheric pressure time series is shown. (For interpretation of the references to colour in this figure legend, the reader is referred to the Web version of this article.)

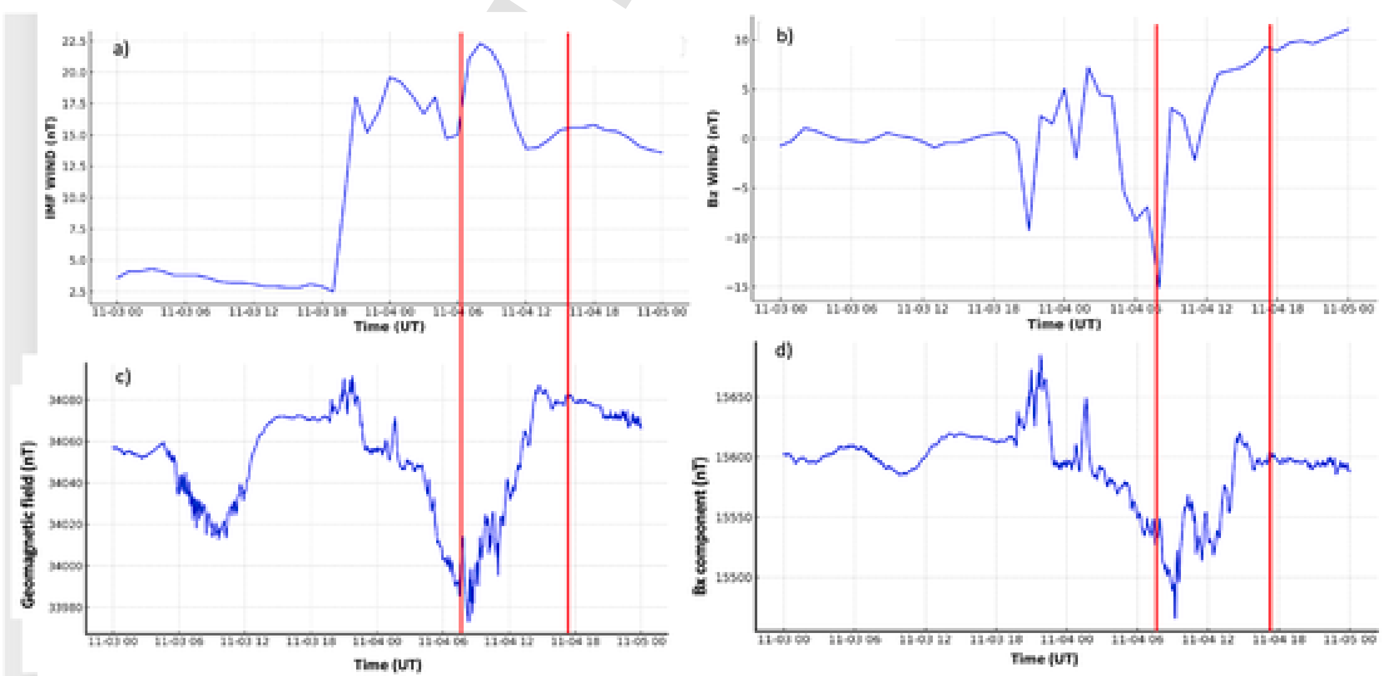

Fig. 3. a) Scalar IMF B; b) IMF Bz component; c) and d) geomagnetic field and its Bx component. Red lines show the depletion phase of FD. (For interpretation of the references to colour in this figure legend, the reader is referred to the Web version of this article.)

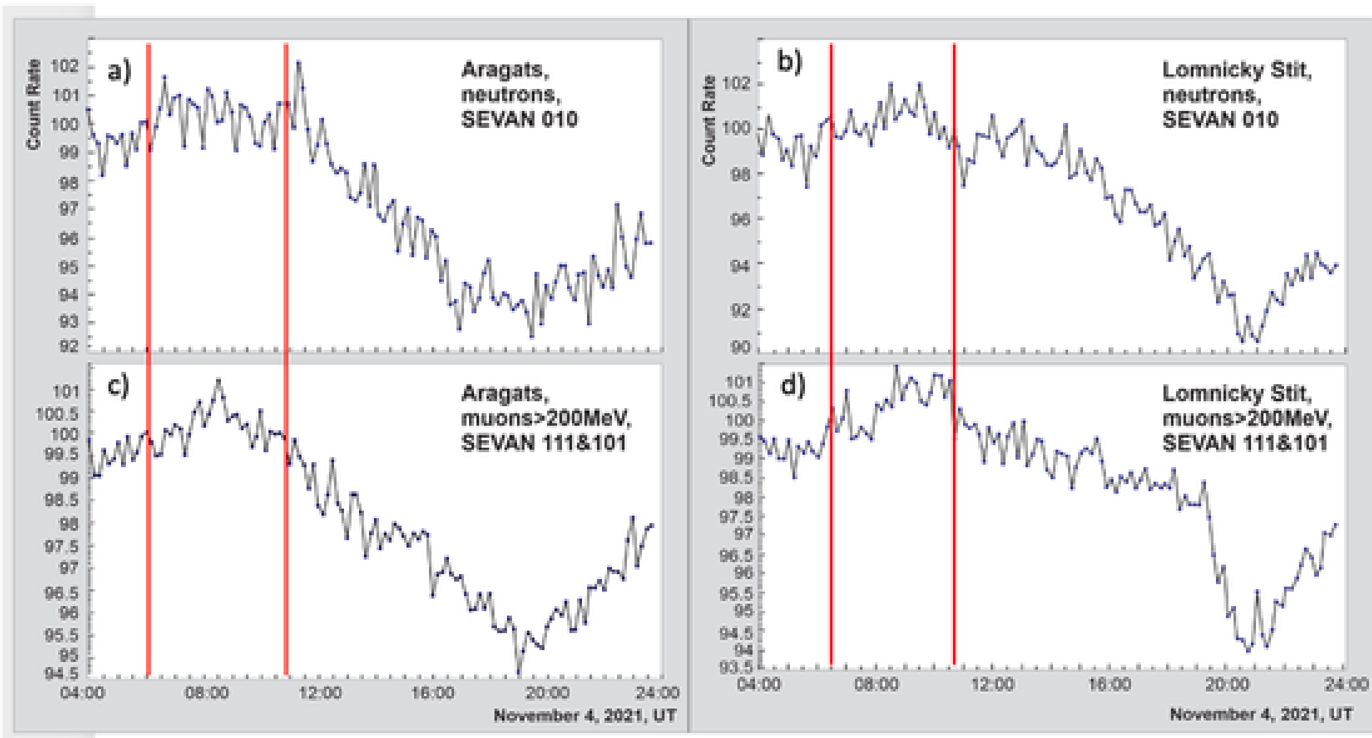

Fig. 4. Ten-minute time series of count rates measured at Aragats and Lomnicky Stit by joint SEVAN 111 + 101 coincidences; muons with energies > 200 MeV. Red lines show the pre-FDs registered on both stations. (For interpretation of the references to colour in this figure legend, the reader is referred to the Web version of this article.)

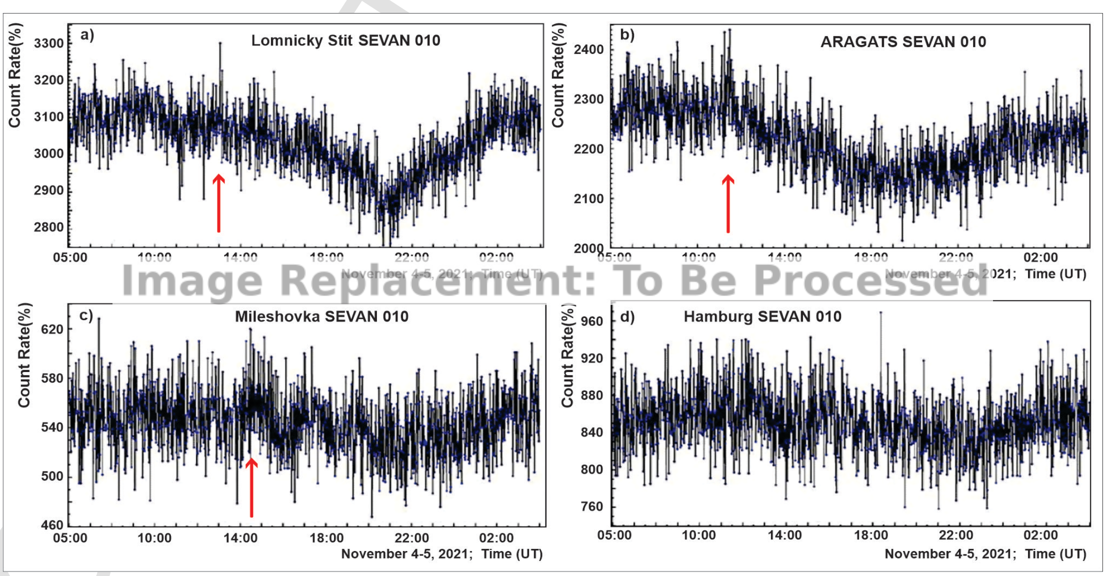

Fig. 5. Pressure-corrected 1-min time series of count rates of "010" coincidence of SEVAN layers (primarily neutrons). We show the "pre-Forbush" count rate enhancement by red arrows followed by FD at high-altitude detectors (not seen at sea level). (For interpretation of the references to colour in this figure legend, the reader is referred to the Web version of this article.)

tral secondary particles born in cascades originating in the atmosphere by nuclear interactions of protons and nuclei accelerated in the Galaxy and near the Sun. The SEVAN network is compatible with the currently operating Neutron monitor network (Mishev and Usoskin, 2020) ''Spaceship Earth" (Kuwabara et al., 2006), coordinated by the Bartol Research Center, the Solar Neutron Telescopes (SNT) network coordinated by Nagoya University (Muraki et al., 1995), the Global Muon Detector Network (GMDN) (Munakata et al., 2000; Rockenbach et al., 2011), and the Neutron Monitor Data Base (NMDB , Mavromichalaki et al., 2011, http://www. nmdb. eu/). The analogical detector operates in China (Tibet: 30.11N, 90.53E, altitude 4300 m, Zhang et al., 2010).

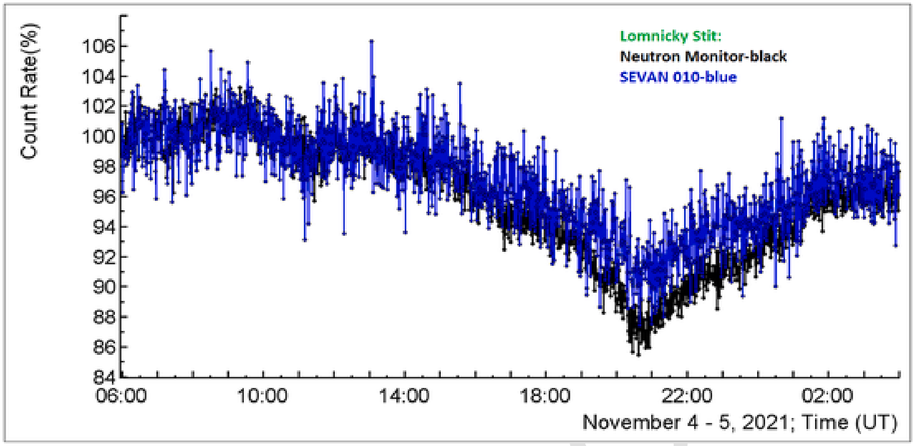

Fig. 6. 1-minute time series of count rates of Neutron Monitor (black) and SEVAN's "010" (primarily neutrons) coincidence, both located at Lomnicky Stit.

Three SEVAN detectors are operating in Armenia (on the slopes of Aragats Mt.: 40.25N, 44.15E, altitudes 1600 m, 2000 m, 3200 m), one detector in Croatia (Zagreb observatory: 45.82N, 15.97E, altitude 120 m), one detector in Bulgaria (Mt. Musala: 42.1N, 23.35E, altitude 2930 m), one detector in Slovakia (Mt. Lomnicky Stit: 49.2N, 20.22E, altitude 2634 m, one detector on Mileshovka hill (50.6N, 13.9E, altitude 837 m) in the Czech Republic, one detector on Zugspitze Schneefernerhaus (47.42N, 10.98E, altitude 2650 m), and one detector in DESY Hamburg (53.5730N, 9.8810E, altitude 20 m). The potential recipients of SEVAN detectors are the USA, Italy, Israel, France, and Algeria.

Just in the first years of the SEVAN network operation, we have recognized that not only solar activity modulates the fluxes of secondary cosmic rays but also various effects in the terrestrial atmosphere and ionosphere. During thunderstorms, emerging strong electric fields modulate the secondary particle energy spectra, initiating short and extended bursts. The impulsive enhancements of the particle fluxes (so-called thunderstorm ground enhancements –TGEs, Chilingarian et al., 2010) are disclosed as peaks in the time series of count rates of particle detectors coinciding with the strong atmospheric electric field, which accelerates and multiplies free electrons of cosmic rays. The physics of particle burst phenomena, connected to the EAS phenomenon and complicated atmospheric processes, is now called high-energy physics in the atmosphere (HEPA). Solar, astroparticle, and atmospheric physics are synergistically connected and need to exchange results for the explanation of particle bursts and for revealing the influence of solar flares, explosions in the galaxy and beyond, as well as the impact of the atmospheric electric fields on the fluxes of secondary cosmic rays registered on the Earth's surface.

The synergy of all high-energy astrophysics branches will open new research areas for better understanding and developing physics of the geo-space. Geophysical research is becoming increasingly important in the coming decades of rapidly rising natural disasters.

2. SEVAN detector

The basic detector of the SEVAN network (Fig. 1a, see Chilingarian et al., 2018) consists of standard slabs of 50 x 50 $\times$ 5 cm^3 plastic scintillators. Between two identical assemblies of 100 x 100 $\times$ 5 cm^3 scintillators (four standard slabs), two 100 x 100 $\times$ 5 cm^3 lead absorbers are positioned, and a thick 50 x 50 $\times$ 25 cm^3 scintillator stack (5 standard slabs). Scintillator lights capture cones, and PMTs are located on the detector's top, bottom, and intermediate layers. The total weight of the SEVAN detector, including steel frame and detector housings, is ≈ 1,5 tons.

Data Acquisition (DAQ) electronics provide registration and storage of all logical combinations of the detector signals for further offline analysis and for online alerts issuing, thus allowing the registration of 3 species of incident particles. If we denote by ''1″ the signal from a scintillator and by ''0″ the absence of a signal, then the following combinations of the 3-layered detector output are possible: 111 and 101—traversal of high energy muon; 010—traversal of a neutral particle; 100—traversal of low energy charged particle stopped in the scintillator or the first lead absorber (energy less than ≈100 MeV). 110—traversal of a high-energy charged particle stopped in the second lead absorber. 001—registration of inclined charged particles. The Data Acquisition electronics (DAQ) allows the remote control of the PMT high voltage and other detector parameters.

On April 2023we installed modernized SEVAN-light detector at the Umwelt-Forschungs-Station (UFS, Schneefernerhaus, 2650 m asl, see Fig. 1b) near the top of the Zugspitze (2962 m), a site with a long history of atmospheric research, where Joachim Kuettner did his seminal experiments on the structure of the electric field in the lower atmosphere (Kuettner, 1950). Due to the building constraints at UFS, SEVAN-light should be compact, shorter, and much lighter than the basic SEVAN. Thus, SEVAN-light consists only of 2 layers, and the lead absorber is not included (total weight ≈ 100 kg). However, we added a modernized electronics board with a logarithmic amplitude-to-digit-converter (LADC), which provides particle energy spectrum recovery in the range of 0.3–100 MeV. This option allows for the first time to measure the energy spectrum of additional particles caused by the magnetospheric effect (Chilingarian et al., 2024).

The SEVAN-light is also fully operational for high-energy atmospheric physics research, with the additional feature of measuring the energy spectrum of TGE particles. The cosmic ray variation studies, related to research in solar physics and space weather domains, will also be continued with low-energy charged and neutral particles and their energy spectra.

In Table 1, we present the purity of the particle detector flux observed by different coincidences of the SEVAN detector. As we can see from Table 1, the "010" coincidence efficiently selects neutrons (52%) and gamma rays (28%), the "111" coincidence muons (96%), and the "100" coincidence low–energy muons and electrons (75%).

3. Particle flux correction to atmospheric pressure

The correction to atmospheric pressure (barometric effect) is usually made to disentangle the atmospheric pressure and solar modulation (sometimes relatively weak) effects on particle flux intensity. Barometric coefficients were calculated for the SEVAN detector on Aragats

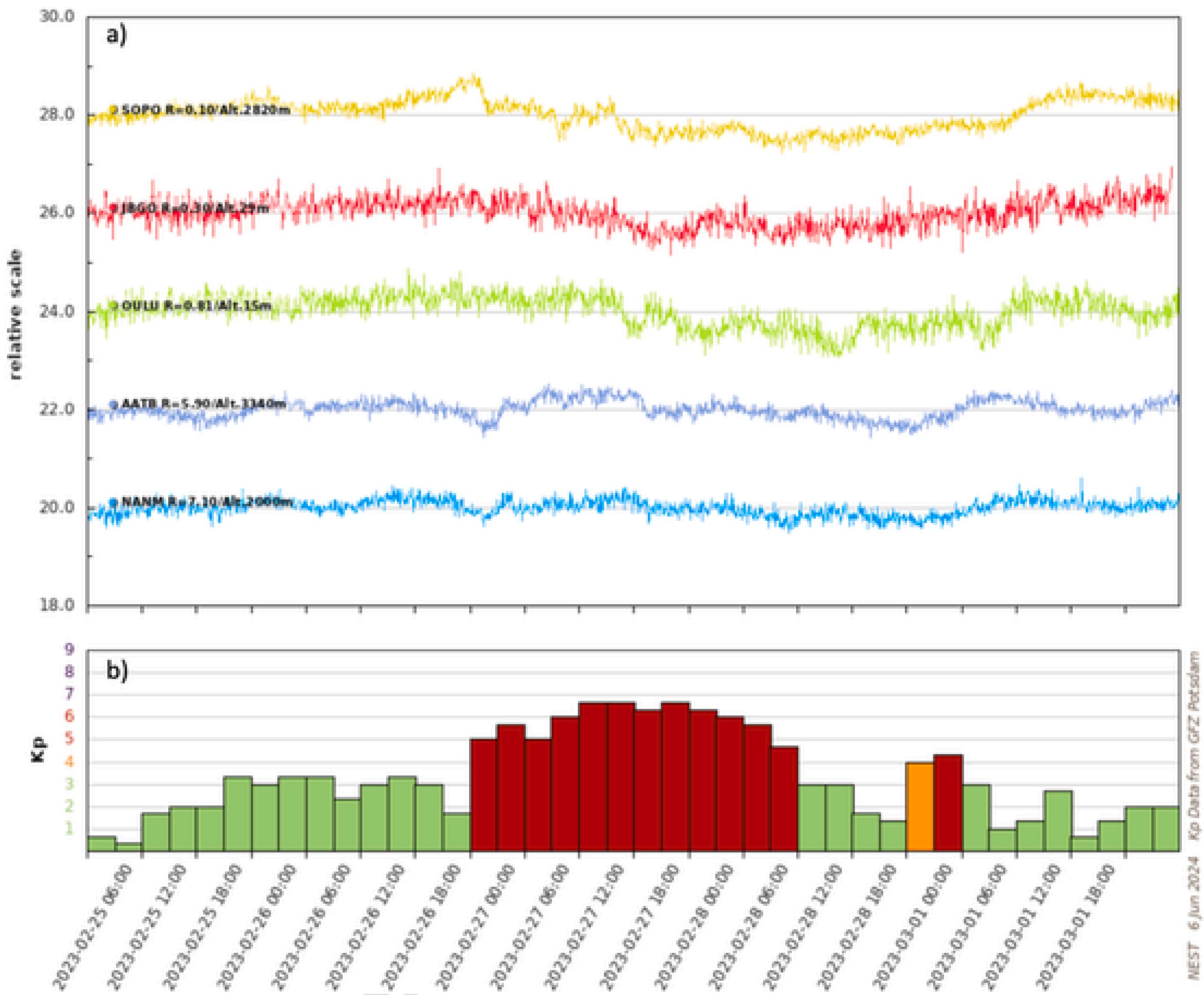

Fig. 7. a) Time series of count rates of the mountain and sea-level neutron monitors; b) Kp indices measured by surface magnetometers.

and other SEVAN sites, using a time series of 1-min pressure data measured by the wireless Vantage Pro2TM plus weather station. On October 26-28, 2018, the 19 mb total change in the atmospheric pressure was measured. The estimate of the barometric coefficient was found by the linear correlation between the intensity of the cosmic ray flux and corresponding data on atmospheric pressure (Dorman, 1974; Chilingarian and Karapetyan, 2011). The least square method was used to obtain the regression coefficients.

In Table 2, we show the barometric coefficients calculated for the Aragats SEVAN detector. The columns posted the altitude, cutoff rigidity, barometric coefficient, goodness of fit in the form of the correlation coefficient, count rate, "Poisson" estimate of relative error (standard deviation divided by average count rate), and actual relative error. The values posted in the last two columns should be very close to each other, and as can be seen from Table 2, the values are identical. This means the adopted model (linear correlation between atmospheric pressure and count rate plus Gaussian random noise) is correct.

Fig. 2 shows the pressure corrected and uncorrected time series of the SEVAN "010" coincidence and the atmospheric pressure time series.

4. Forbush decrease measured by SEVAN network

The solar wind routinely modulates the flux of low-energy GCRs, changing the structures and polarities of the local magnetic fields in the heliosphere and magnetosphere. Thus, variations in the intensity of secondary cosmic rays observed at the Earth's surface can provide valuable information on the distribution of these structures in the heliosphere and interactions of the solar wind with the magnetosphere.

The particle fluxes measured on the Earth's surface exhibit depletions (called Forbush Decreases -FDs, increasing the geomagnetic cutoff rigidity) and enhancement (Magnetospheric effect ME, lowering the geomagnetic cutoff rigidity) due to disorders in near-earth magnetic structures as a reaction to propagated shocks and ICMEs. Forbush decreases are the most frequent and easy-to-detect phenomenon of solar modulation of galactic cosmic rays. Historically, more than eighty years ago, Scott Forbush was the first who relate these depletions of cosmic radiation (CR) flux with solar eruptions (Forbush, 1954).

When observed with networks of particle detectors, FDs usually exhibit a highly asymmetrical structure: a fast decrease of the flux with a time scale of some hours, followed by a smooth recovery with a time

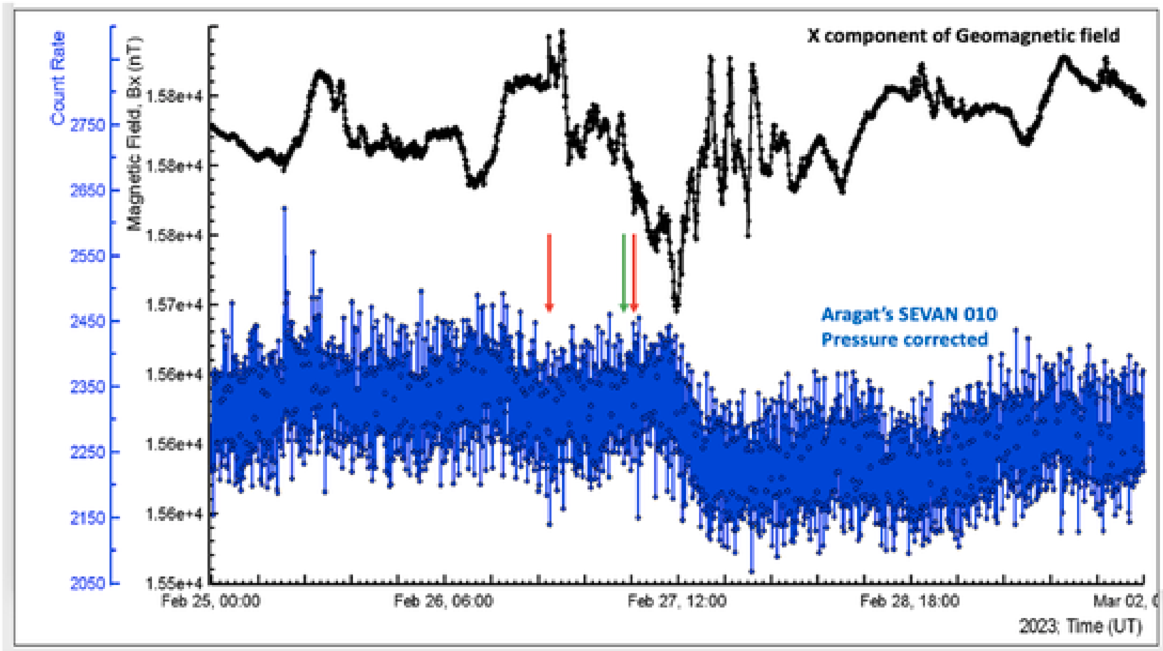

Fig. 8. The disturbances of the X component of the geomagnetic field and pressure corrected data of the SEVAN 010 coincidence. The ICME arrivals are shown by red arrows and the start of the G3 geomagnetic storm by the green arrow. (For interpretation of the references to colour in this figure legend, the reader is referred to the Web version of this article.)

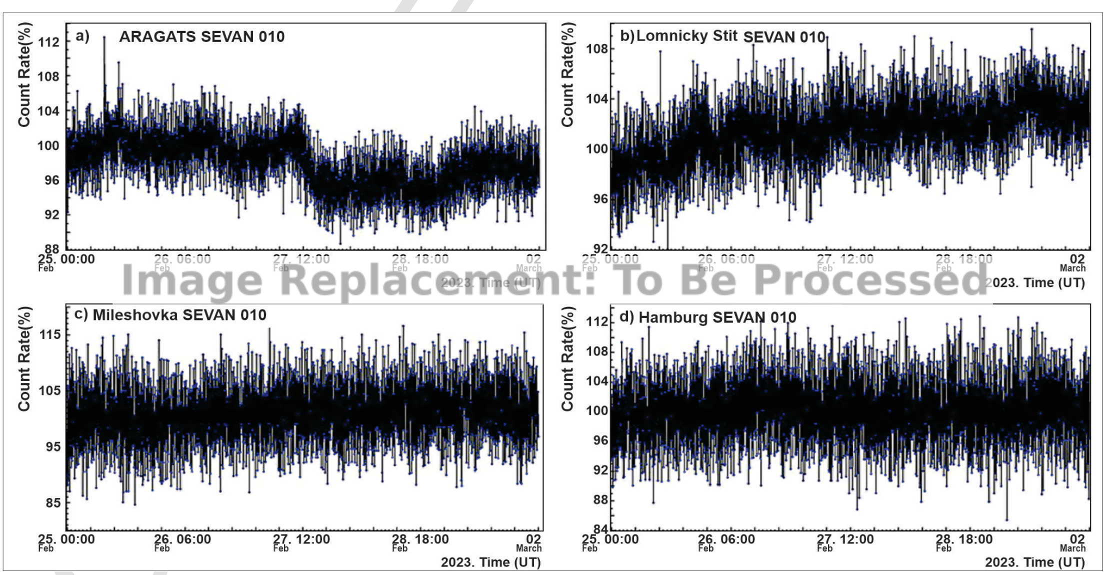

Fig. 9. FD registered on February 27, 2023 by the Aragats' SEVAN and missed by European SEVANs.

scale of several days. Suppose episodes of solar bursts follow each other (usually from the same active region). In that case, multiple fast waves of magnetized solar plasma travel simultaneously through interplanetary space, sometimes overtaking each other (referred to as "cannibalism") and arriving at 1 AU as a complex magneto-plasmatic structure. Usually, these complex structures contain enhanced southward magnetic field components, which is a critical factor in generating geomagnetic storms (Maričić et al., 2014). Thus, FDs can have relatively complex anisotropy structures demonstrating consequent depletions without a recovery stage, like the Halloween events of 2003 (Chilingarian et al., 2003).

Cosmic ray flux typically shows pre-increases by about 1–2 % because cosmic rays are reflected on the approaching solar wind shock. When the shock wave from fast solar wind reaches Earth's magnetosphere, in most cases, an abrupt change in the geomagnetic field, named sudden storm commencement (SSC), is detected, then starts the main decrease phase caused by the solar winds/ejecta's southward magnetic field. Then, a recovery phase finalizes FD. The intensity of the GMS is measured by the disturbance storm time index (DST) and symmetric H-component (SYM-H), which gauge the intensity of the ring current using low-latitude ground-based magnetometers measurement. In the present study, we have used Internet-based Operating missions as nodes

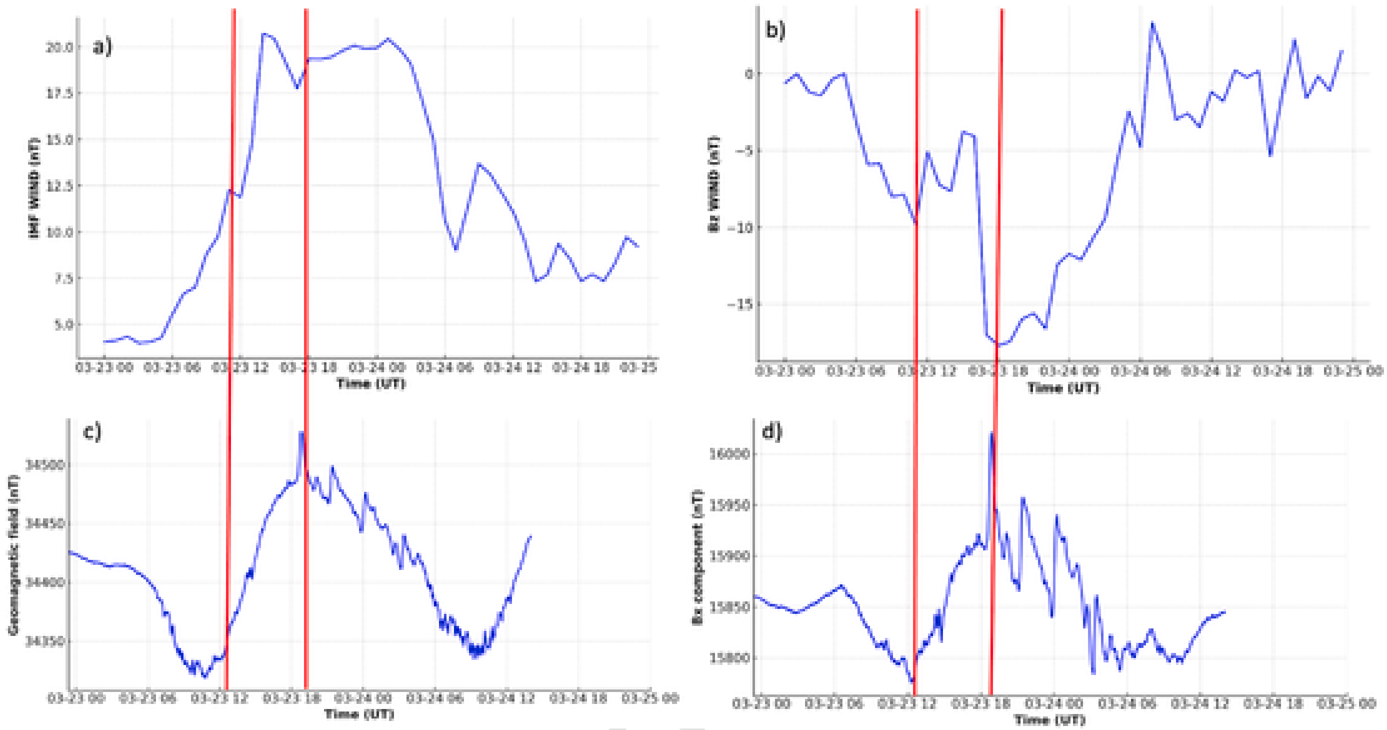

Fig. 10. a) Scalar IMF B; b) IMF Bz component; c) and d) geomagnetic field and its Bx component. Red lines show the depletion phase of FD. (For interpretation of the references to colour in this figure legend, the reader is referred to the Web version of this article.)

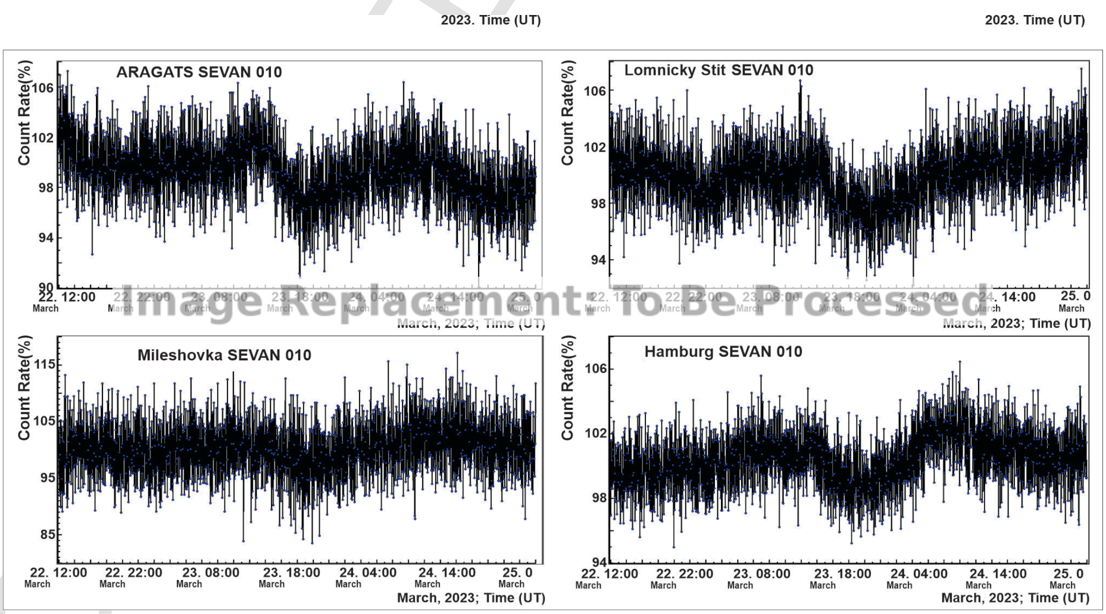

Fig. 11. FD registered on March 23, 2023 by the SEVAN network.

on the Internet web system (OMNI, https://omniweb.gsfc.nasa.gov/ow.html). We obtain the interplanetary magnetic field B and southward component Bz from the WIND satellite magnetometer via the OMNI system.

Measurements of the FD magnitude in the fluxes of different secondary CR species reveal significant correlations with speed, size of the ICME, and the ‘‘frozen’’ in ICME magnetic field strength (Chilingarian and Bostanjyan, 2010). Measurements of all the secondary cosmic-ray fluxes at the same location are preferable due to the effects of the longitudinal dependence of the FD magnitudes (Haurwitz et al., 1965). The research of the diurnal variations of GCR by the observed fluxes of charged and neutral secondary CR also opens possibilities to correlate the changes of parameters of the daily wave (amplitude, phase, maximal limiting rigidity) with the energy of GCRs (Mailyan and Chilingarian, 2010). An example of a practical application of surface CR measurements, including FD, is given by (Kakona et al., 2016).

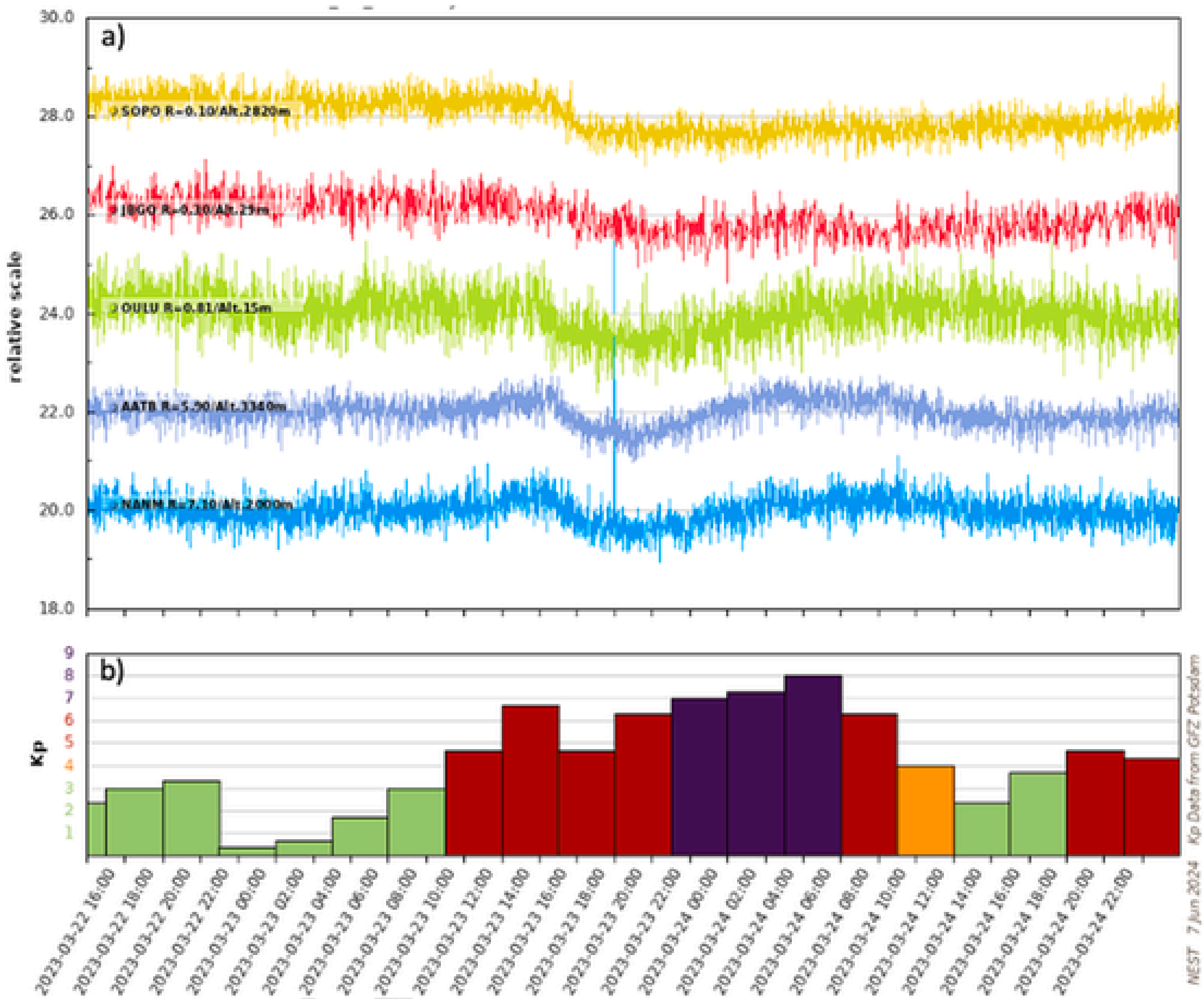

Fig. 12. a) FD registered on March 23, 2023 by the NM network; b) Kp indices measured by surface magnetometers.

On 3–5 November 2021, a large GMS unleashed auroras as far low latitude as New Mexico (39N)! SOHO coronagraphs caught the storm cloud leaving the Sun on 2nd November, following and overtaking the previous slower-moving solar flare (M1.7) in the magnetic canopy of sunspot AR2891. As the "cannibal" ICME approaches and passes the satellites at the L1 point on 4th November, the IMF got large values approaching and exceeding 20 nT (Fig. 3a); the Bz component of the IMF dipped −15 nT at 8:00 UT and turned to positive domain afterward (Fig. 3b). The geomagnetic field measured at Aragats station by LEMI-417 sensor was changed coherently, reaching a minimum at 11:08 UT (Fig. 3c); the Bx component after large disturbances reaches a minimum (compressed by the solar wind) at 11:09 (Fig. 3d). Thus, the depletion phase of FD, outlined in Fig. 3 by red lines coincides with the largest values of IMF, fast changing values of Bz, and compression of the magnetosphere (the lowest values of the Geomagnetic field and its Bx component).

The FD started with a significant pre-FD increase, which lasted nearly 4.5 h from 6:00 to 10:00 on Aragats and nearly 4 h from 6:30 to 10:30 on Lomnicky Stit, see Fig. 4.

Mountain SEVAN detectors coherently registered a pre-FD increase in fluxes of high-energy muons ($E\mu >$ 200 MeV, SEVAN coincidence 111 & 101, muons traversing 10 cm of lead). After pre-FD, the SEVAN network registered the FD main phase on Aragats, Lomnicky Stit, Mileshovka, and Hamburg. Fig. 5 shows FD in a 1-min time series of count rates of the "010" coincidence (mostly neutrons). The FDs at mountain altitudes (Aragats, Lomnicky Stit, all above 2500 m) are pronounced better than at lower altitudes (Mileshovka, ≈800 m) and sea level (Hamburg and Berlin, see Fig. 5).

In Fig. 6, we compare FD registration by the Neutron Monitor and the "010" coincidence of the SEVAN detector, located in the same place at Lomnicky Stit. The correlation of both is perfect, although the FD amplitude measured by NM is larger than that of SEVAN.

5. Forbush decreases of 26–28 February observed by SEVAN Aragats detector and neutron monitors

Full hallo SMS from solar flares on February 25 and 26 (M3.7 and M6.2 from Active Region 2329) arrived at 18:30 UT on February 26 and 10:00 UT on February 27. A global network of real-time magnetometers

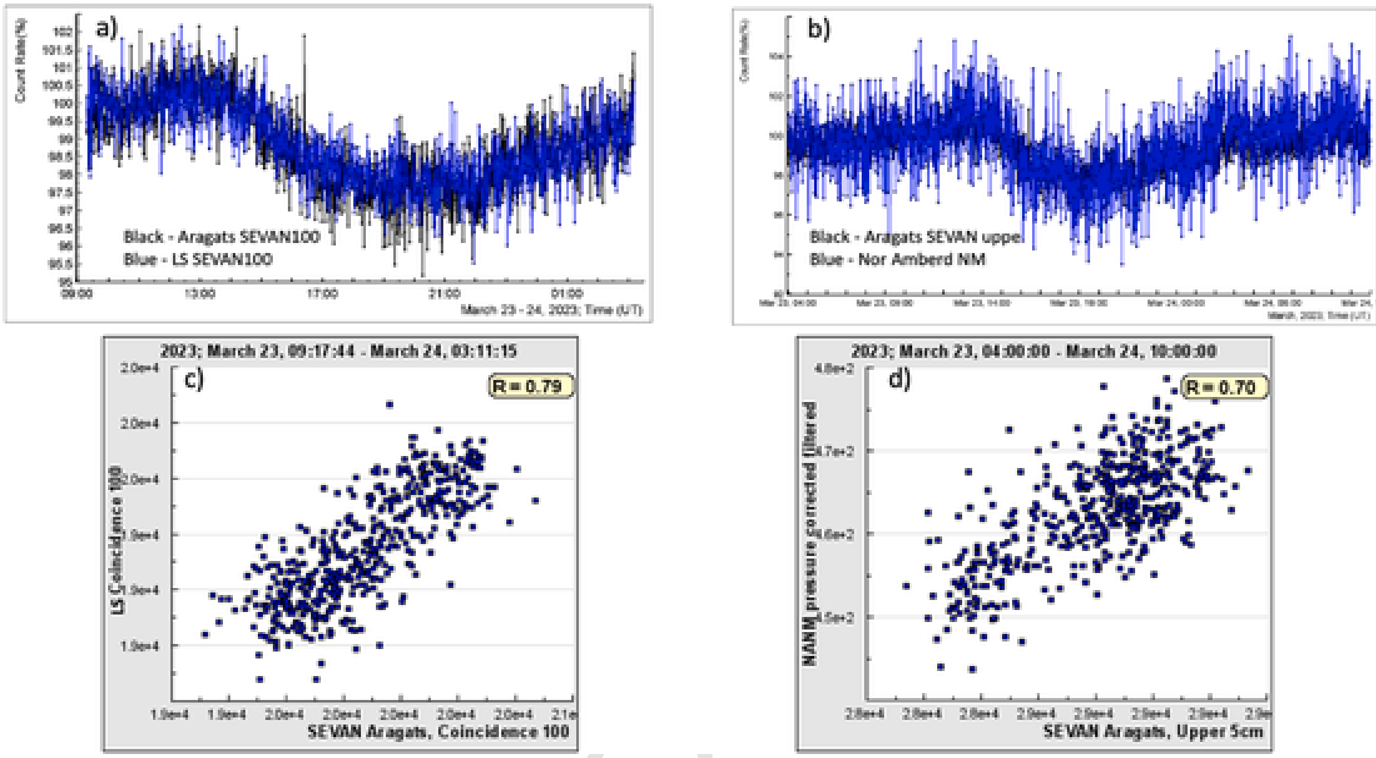

Fig. 13. a) time series of count rates of SEVAN "100" coincidences measured on Aragats and at Lomnicky Stit; b) the same from Aragats and Nor Amberd neutron monitor; c) and d) scatter plots of variables depicted in frames a) and b).

reported the G3 GMS started on Feb 27 at 6:00 UT. The particle event was prolonged and highly anisotropic, as shown in Fig. 7a. Intensity variations were observed for three days from February 26, 18:00 to 28 6:00, see Fig. 7b. The high-altitude Antarctic station SOPO first registered particle flux enhancement followed by 2-day sporadic depletions. Another Antarctic monitor, JBGO (sea-level), does not measure any enhancement, only a smooth depletion a day after SOPO's enhancement. European sea-level monitor (OULU) exhibits sporadic depletions after noon on 27 February. Correlated depletion was observed at Aragats and Alma-Ati monitors.

Fig. 8 shows a 1-min time series of the SEVAN's 010 coincidence (mainly neutrons) and disturbances of the X component of the geomagnetic field. The first depletion of count rate on 26 February is related to the arrival of the first ICME, and the second larger depletion at 12:00–18:00 – to the second ICME arrival.

European SEVANs do not show any significant features in the time series on February 26–27; see Fig. 9. We attribute these anisotropic and prolonged cosmic ray intensity variation events to large disturbances of the magnetosphere due to the arrival of 2 ICMEs, which pose difficulties in galactic cosmic ray arrival into the atmosphere.

6. Forbush decrease suddenly occurred on March 23, 2023, G1 geomagnetic storm turned to G4

Observed on the 23rd of March by SEVAN nodes, FD was primarily due to a coronal hole high-speed stream (CH HSS) opened for 8 h and from a CME that left the Sun on the 20th of March. A co-rotating interaction region (CIR) with the relatively slower ambient solar wind forms a compression region ahead of the HSS. Finally, the disturbances in the solar wind resulted in a strong geomagnetic storm observed at 14:49 UTC on the 23rd of March. Fig. 10a shows IMF got a large value of 20 nT during FD; the Bz component of the IMF dipped −18 nT from -5nT during the depletion phase of FD (Fig. 10b). The geomagnetic field, and its Bx component were on minimal value at the start of FD and smoothly enhanced at the end (Fig. 10 c and 10d). Thus, the depletion phase of FD, outlined in Fig. 10 in red lines, coincides with the largest values of IMF and the neagtive values of Bz (directed southward). The largest compression of the magnetosphere (lowest values of the Geomagnetic field and its Bx component) was at the start of FD, considerably enlarged to the end.

Fig. 11 shows the FD registered by the SEVAN network (coincidence 010, mostly neutrons), and Fig. 12 shows the NM network's FD. The development of FD registered by detectors of both networks shares similar features: a pre-FD increase, amplitude of 4–5%, a 5-h duration of the depletion phase, and a short recovery phase.

SEVAN and NM detectors operated at Lomnicky Stit and Aragats high-altitude research stations. Both types of detectors demonstrate coherent depletion and recovery of cosmic ray fluxes. The data of these NMs and more than 40 NMs worldwide are entering the NMDB database (Mavromichalaki et al., 2011). The data from SEVAN detectors are stored at Aragats servers and are available via multivariate visualization and correlation analysis platforms (Chilingarian et al., 2008, Chilingrayan et al., 2010). Thus, we can compare remote measurements of FD with the same type of detectors and measurements of the different types of detectors sensitive to different types of secondary cosmic rays, such as muons and neutrons. Fig. 13a shows the time series (in percent to undisturbed value) of the count rates of the "100" coincidence of Aragats and Lomnicky Stit SEVAN detectors (mostly muons and electrons; see Table 1). Fig. 13b shows the time series of the count rates of Aragats SEVAN and Nor Amberd neutron monitor. Fig. 13 c and 13d show the scatter plot of the variables depicted in the upper plots and the correlation coefficients. The correlation coefficient of remote detectors registering charged and neutral particles are significantly high, proving the equivalence of charged and neutral species of secondary particles in FD. Thus, this FD was uniform, robust, and independent of particle types and geographical coordinates.

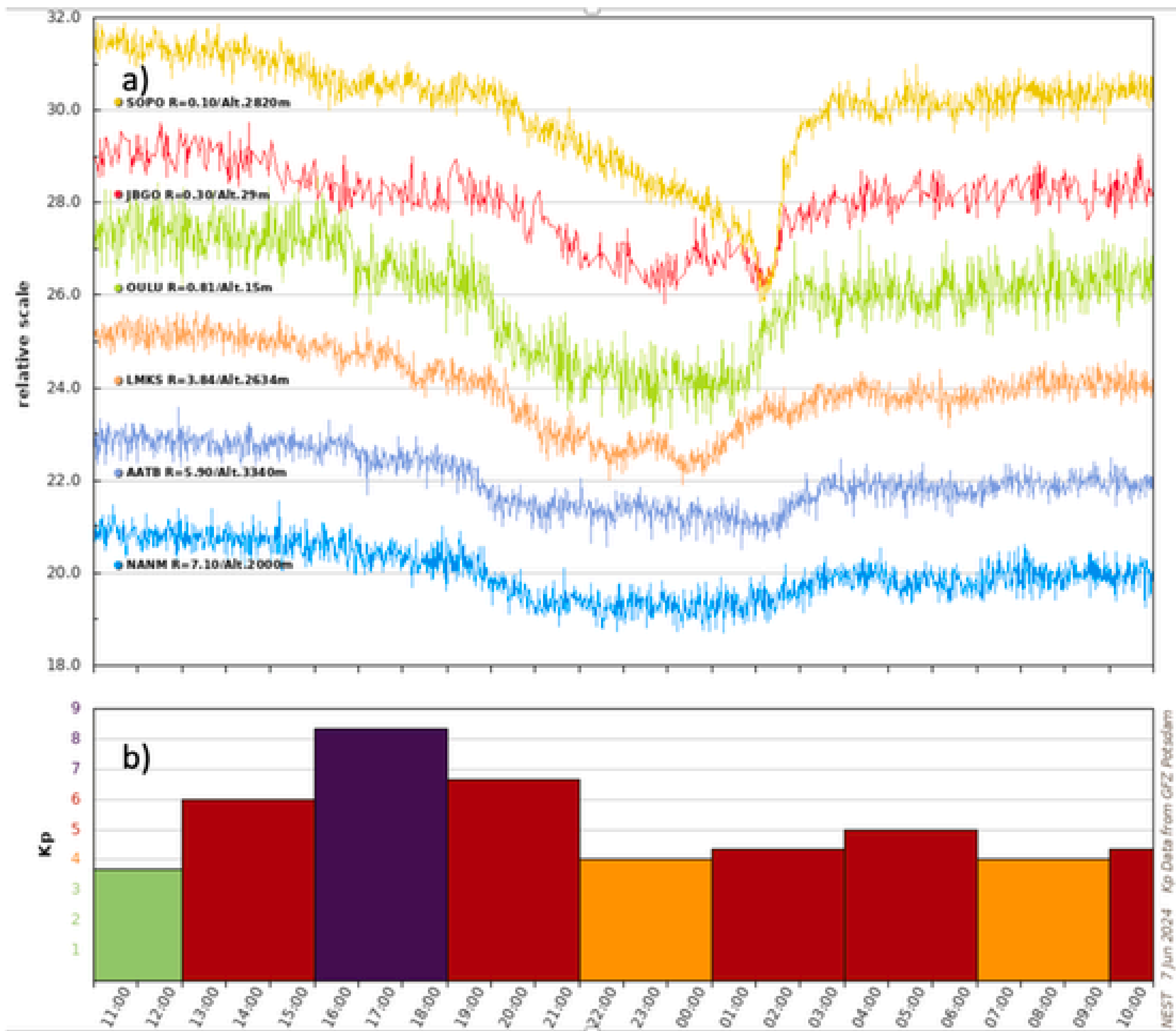

Fig. 14. a) FD registered by the NM network from the Antarctic to North Europe; b) Kp indices measured by surface magnetometers.

7. Forbush decrease of March 24, 2024, caused by sympathetic flares

The long-duration X1.1-class flare started on the 23rd of March, around 01:30 UT when AR3614 and AR3615 erupted. NASA's Solar Dynamics Observatory recorded the double blast, a "sympathetic solar flare." Sympathetic flares occur almost simultaneously in widely spaced sunspots due to an unseen physical connection. Magnetic loops in the sun's corona connect some sunspots, allowing explosive instabilities to travel between them. Some sympathetic flares are so alike they are considered twins. The 23rd March CME arrived at the Earth around 14:11 on the 24th of March, leading to a G4-class geomagnetic storm, one of the most potent since 2017. This storm caused disruptions in satellite operations and communication systems. It launched a peculiar FD with a very short recovery phase, observed by NM (Fig. 14) and SEVAN particle detector networks (Fig. 15). Neutron monitors with low cutoff rigidity (SOPO, OULU) demonstrate larger FD amplitudes. The Antarctic high-altitude monitor (SOPO) demonstrates much deeper FD than the sea level monitor (JBGO). However, in Europe, FD registered by sea level OULU monitor was deeper than mountain monitors (LMKS, AATB, and NANM). Thus, the cutoff rigidity was more important than altitude. We can conclude that a disturbed magnetosphere influences not only the lowest energy galactic protons (as at magnetospheric effect, Chilingarian et al., 2024) but also intermediate ones.

Fig. 15 shows exact correlated count rates measured by geographically neighboring SEVAN detectors in Eastern Europe, at the mountains Lomnicky Stit, Zugspitze, and Milesovka, near Prague. The FD pattern is almost the same, amplitude 5–6% (Fig. 15a), and correlation coefficients between all pairs are very significant (Fig. 15 b-d). The FD shapes of SEVAN detectors are also very similar to shapes measured by neutron monitors at the same destinations. It proves the equivalence of neutron and muon content in FD registration.

Fig. 16 shows that the IMF got large values approaching and exceeding 30 nT during FD (Fig. 16a); the Bz component of the IMF dipped at −12 nT at the FD start and then peaked at 15 nT (Fig. 16b). The geomagnetic field measured at Aragats station was highly dis-

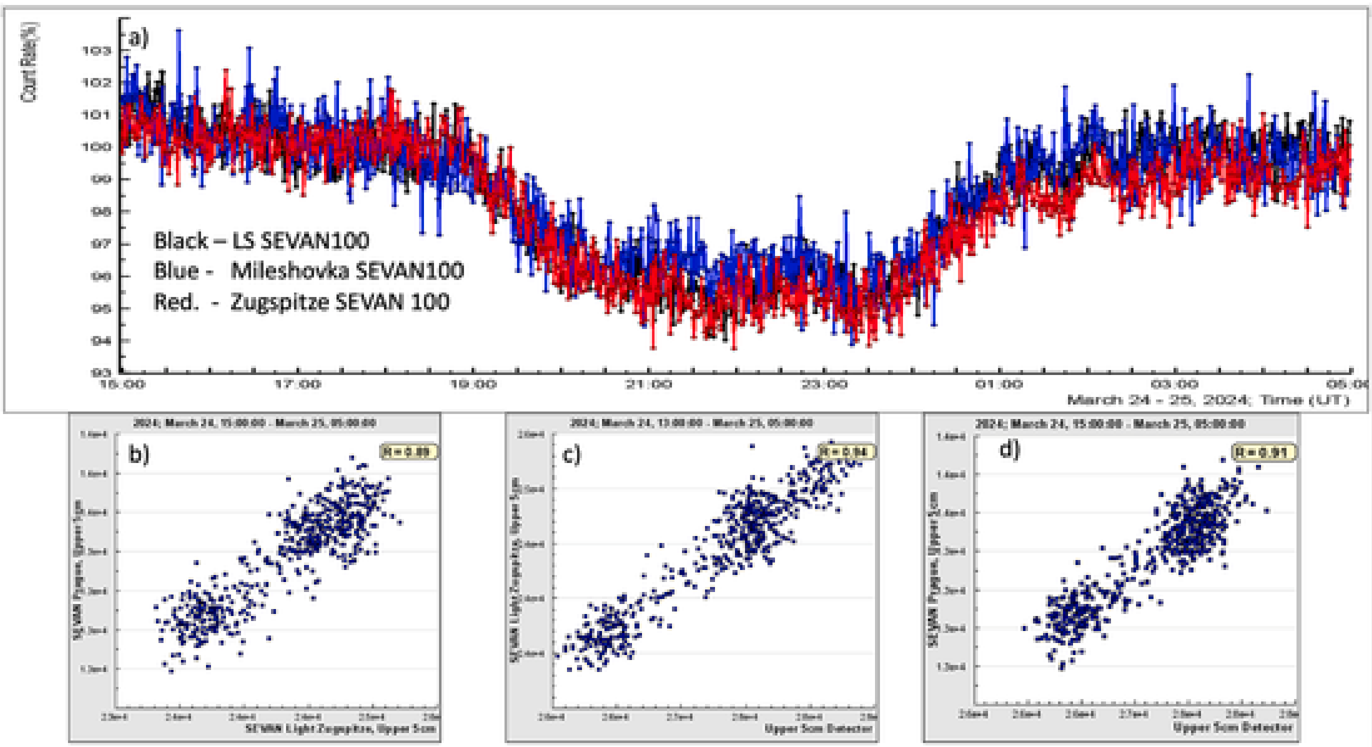

Fig. 15. a) Time series of count rates of SEVAN 100 coincidence (mostly muons and electrons); b-d) pair-wise scatter plots of measurements by 3 SEVAN detectors.

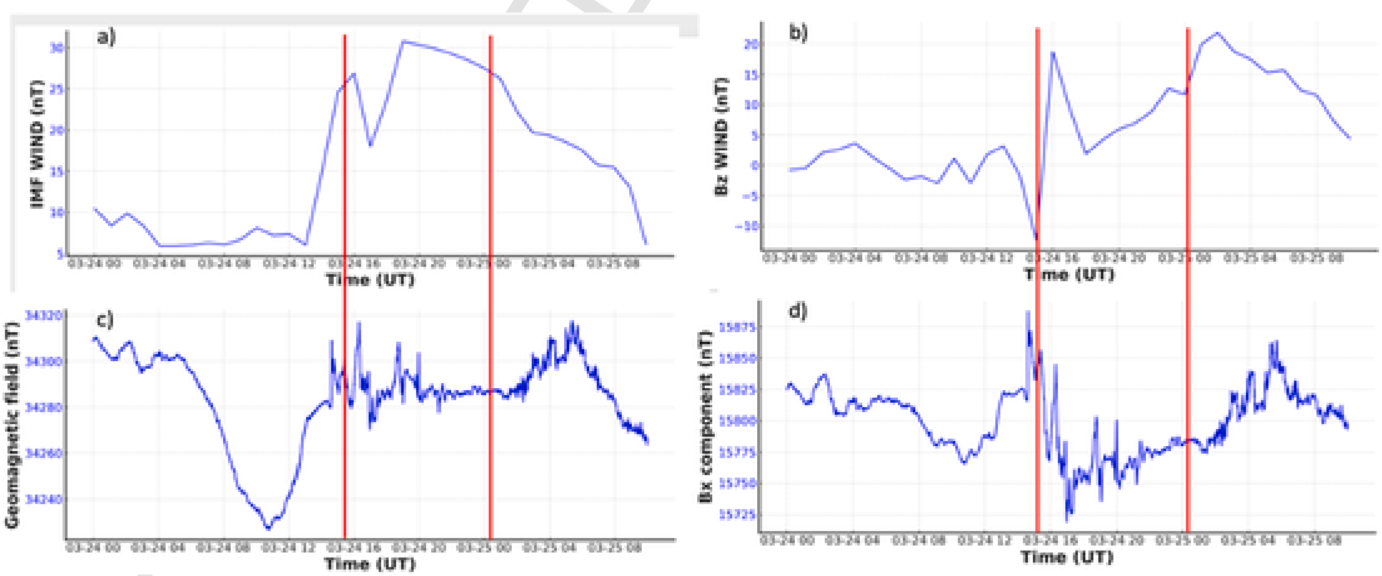

Fig. 16. a) Scalar IMF B; b) IMF Bz component; c) and d) geomagnetic field and its Bx component. Red lines show the depletion phase of FD. (For interpretation of the references to colour in this figure legend, the reader is referred to the Web version of this article.)

turbed during FD (Fig. 16c and d); the solar wind compressed the Bx component. Thus, the FD, outlined in Fig. 16 by red lines, coincides with the largest values of IMF, variate values of Bz, and large compression of the magnetosphere.

8. Discussion and conclusions

In Chilingarian & Bostanjan (2009), we statistically analyzed FD detected by Aragats particle detectors during the 23rd solar cycle. We found that FD amplitude depends on factors such as CME launch coordinates, a fast shock, ICME density, the frozen magnetic field, and magnetospheric conditions disturbed by previous ICMEs. Our study in concluded that FD can be successfully studied in charged particle fluxes,

Table 3
Characteristics of Solar particle events at approaching the maximum of 25ths Solar cycle.

Date/time	Duration (depletion phase)	Event type	Kp	-% of flux change	IMF nT	Bz nT	Bx % Depletion
November 4, 2021	10:30–13:30	FD	5–6	8–9	−10 - +40	−20 - +20	−0.5
February 27, 2023	15:00–19:00	FD	5–6	3	+15 to −7	−14– −5	0
March 23, 2023	14:00–18:00	FD	5–6	5–6	+5 - +20	0–−10	0
March 24, 2024	18:30–01:30	FD	8–4	5–6	+20 - +40	−10 - +18	−0.5

with the ratio of neutral to charged flux increases being relatively constant across varying GM severities and neutral flux showing more significant changes.

The SEVAN network, compatible with the NM network, demonstrated consistent FD measurements in different secondary cosmic ray fluxes. The time to reach the FD minimum was similar for mountain peak locations but varied slightly at sea level. The FD amplitudes measured by SEVAN detectors at Aragats and Lomnicky Stit were comparable, indicating isotropic FDs. SEVAN's advantage is measuring FDs in fluxes of different particles with various energy thresholds, showing strong correlations with the geo-effectiveness of solar events.

Collaborative efforts within the SEVAN network, supported by the ADEI data analysis platform, have significantly improved our understanding of the physics of violent solar events. Modernized SEVAN electronics, enabling the measurement of energy spectra of neutral and charged particles, will reveal the populations of solar protons responsible for FD, ME, and GLE.

Table 3 summarizes the described 4 FD events, all coinciding with large GMS. The first two columns display the date and time of the FD depletion phase. The third column indicates the type of solar event, while the fourth column shows the maximum Kp index just before or during FD. The fifth column presents the mean percentage change in particle flux measured by the mountain SEVAN detectors' 100 coincidence (charged particles). The sixth column shows the total magnetic field (IMF). The seventh column displays the values of the z component of the ejecta magnetic field measured during the event by the WIND satellite magnetometer. The last column displays the depletion of the Bx component of the GM field measured by the Aragats magnetometer.

Table 3 confirms that FD depends highly on the disturbed IMF rather than its Bz component. For all FDs, the IMF value was large during the FD depletion. Large IMF interactions with the magnetosphere create traps and cradles for galactic protons and nuclei, preventing their penetration into the atmosphere. The Bz component varies highly, changing from southward to northward. The Bx component of the geomagnetic field, showing the solar wind's compression of the southward magnetosphere, was highly disturbed, indicating a weakening trend. This differs from the magnetospheric effect (ME, Chilingarian et al., 2024) measured during strictly southward Bz and compressed GM field.

Uncited references

; ; ; Chilingarian et al., 2003; ; Chilingaryan et al., 2010; Kuettner, 1950; Thompson et al;

CRediT authorship contribution statement

T. Karapetyan: Writing – review & editing, Visualization, Resources, Investigation, Formal analysis, Data curation. **A. Chilingarian:** Writing – review & editing, Writing – original draft, Supervision, Project administration, Methodology, Investigation, Funding acquisition, Formal analysis. **G. Hovsepyan:** Investigation, Formal analysis. **H. Martoyan:** Formal analysis. **B. Sargsyan:** Visualization, Software, Resources, Investigation, Formal analysis. **R. Langer:** Formal analysis, Data curation. **J. Chum:** Investigation, Formal analysis. **N. Nikolova:** Formal analysis, Data curation. **Hristo Angelov:** Formal analysis, Data curation. **Diana Haas:** Data curation. **Johannes Knapp:** Investigation, Funding acquisition, Formal analysis, Data curation. **Michael Walter:** Methodology, Funding acquisition, Formal analysis, Data curation. **Ondrej Ploc:** Formal analysis, Data curation. **Jakub Šlegl:** Data curation. **Martin Kákona:** Methodology, Investigation, Formal analysis. **Iva Ambrožová:** Formal analysis.

Declaration of competing interest

The authors declare that they have no known competing financial interests or personal relationships that could have appeared to influence the work reported in this paper.

Data availability

Data will be made available on request.

Acknowledgments

We thank the Aragats Space Environmental Center staff (Gurgen Jabaryan, Karen Asatryan, Edik Arshakyan, and others) for the uninterruptable operation of all experimental facilities at high altitude stations We also thank our colleagues from the Neutron Monitor Database (NMDB) and SEVAN collaborations for engaging in valuable discussions. The authors appreciate the support from the Science Committee of the Republic of Armenia, specifically for funding Research Project No. 21AG-1C012. This support was instrumental in modernizing the technical infrastructure of high-altitude stations. The data utilized in this study is accessible through (crd.yerphi/ADEI)in numerical and graphical forms. We also acknowledge the NMDB database (www.nmdb.eu), established under the European Union's FP7 program (contract no. 213007), for providing access to neutron monitor data. The work of the group from the Nuclear Physics Institute of the CAS was supported by the EU Operational Program Research, Development, and Education in project CRREAT (Research Centre of Cosmic Rays and Radiation Events in the Atmosphere) number CZ.02.1.01/0.0/0.0/15_003/0000481.

References

Chilingarian, A., Bostanjyan, N., 2010a. Cosmic ray intensity increases detected by Aragats Space Environmental Center monitors during the 23rd solar activity cycle in correlation with geomagnetic storms. J. Geophys. Res. 114 (A9), A09107.
Chilingarian, A., Bostanjyan, N., 2010. On the relation of the Forbush decreases detected by ASEC monitors during the 23rd solar activity cycle with ICME parameters. Adv. Space Res. 45, 614–621.
Chilingarian, A., Karapetyan, T., 2011. Calculating the barometric coefficients at the start of the 24th solar activity cycle for Aragats Space Environmental Centre particle detectors. Adv. Space Res. 47, 1140.
Chilingarian, A., Hovsepyan, G., Arakelyan, K., et al., 2009. Space environmental viewing and analysis network (SEVAN). Earth Moon Planets 104 (1), 195.
Chilingarian, A., Daryan, A., Arakelyan, K., et al., 2010. Ground-based observations of thunderstorm-correlated fluxes of high-energy electrons, gamma rays, and neutrons. Phys. Rev. D 82, 043009.
Chilingarian, A., Babayan, V., Bostandjyan, N., et al., 2003. Monitoring and forecasting of the geomagnetic and radiation storms during the 23RD solar cycle: Aragats regional space wheather center. Adv. Space Res. 31, 861–865.
Chilingarian, A., Babayan, V., Karapetyan, T., et al., 2018. The SEVAN Worldwide network of particle detectors: 10 years of operation. Adv. Space Res. 61, 2680–2696.
Chilingarian, A., Karapetyan, T., Sargsyan, B., Knapp, J., Walter, M., Rehm, T., 2024. Increase in the count rates of ground-based cosmic-ray detectors caused by the heliomagnetic disturbance on 5 November 2023. EPL. https://doi.org/10.1209/0295-5075/ad329c.
Chilingaryan, S., Beglarian, A., Kopmann, A., Voekling, S., 2010. Advanced data extraction infrastructure: a WEB-based system for time series data management. J. Phys. Conf. Ser. 219, 042034.
Dorman, L.I., 1974. Cosmic Rays, Variations, and Space Exploration. (Amsterdam, North

Holland).

Forbush, S.E., 1954. World-wide cosmic-ray variations in 1937-1952. J. Geophys. Res. 59, 525.

Gevorgyan, N., Avakyan, K., Babayan, V., et al., 2005. Test alert service against very large SEP Events. Advances in Space Research 36 (12), 2351–2356. https://doi.org/10.1016/j.asr.2004.04.016.

Haurwitz, M.W., Yoshida, S., Akasofu, S.I., 1965. Interplanetary magnetic field asymmetries and their effects on polar cap absorption effects and Forbush decreases. J. Geophys. Res. 70, 2977–2988.

Kakona, M., Ploc, O., Kyselova, D., et al., 2016. Investigation of the Contribution of Neutron Monitor.

Kuwabara, T., Bieber, J.W., Clem, J., et al., 2006. Realtime cosmic ray monitoring system for space weather. Space Weather 4, S08001.

Leerungnavarat, K., Ruffolo, D., Bieber, J.W., 2003. Loss cone precursors to Forbush decreases and warning of space weather effects. Astrophys. J. 593, 587–596.

Mailyan, B., Chilingarian, A., 2010. Investigation of diurnal variations of cosmic ray fluxes measured using ASEC and NMDB monitors. Adv. Space Res. 45, 1380–1387.

Maricic, D., Vrsnak, B., Dumbovic, M., et al., 2014. Kinematics of interacting ICMEs and related Forbush decrease: case study. Solar Phys 289, 351–368.

Mavromichalaki, H., Papaioannou, A., Plainaki, C., et al., 2011. Applications and usage of the real-time neutron monitor database for solar particle events monitoring. Adv. Space Res. 47, 2210–2222.

Mishev, A., Usoskin, .I, 2020. Current status and possible extension of the global neutron monitor networkJ. Space Weather Space Clim. 10, 17. https://doi.org/org/10.1051/swsc/2020020.

Munakata, K., Bieber, J.W., Yasue, S., et al., 2000. Precursors of geomagnetic storms observed by the muon detector network. J. Geophys. Res. 105 (A12), 27457–27468.

Kuettner J. 1950. The electrical and meteorological conditions inside thunderclouds, J. Meteorol. 7, 322. doi.org/10.1175/1520-0469(1950)007<0322:TEAMCI>2.0.CO;2

Zhang, J.L., Tan, Y.H., Wang, H., et al., 2010. The yangbajing muon- neutron telescope. NIMA 623, 1030–1034.

Thompson, B.J., Gopalswamy, N., Davila, J.M., Haubold, H.J. (Eds.),. Putting the ''I'' in IHY: the United Nations Report for the International Heliophysical Year 2007. Springer, Wien-New York.

Muraki Y, Sakakibara S., Shibata S., et al (1995). New Solar Neutron Detector and large Solar Flare Events of June 4th and 6th, 1991, J. Geomag. Geoelectr., 47 (1995) 1073-1078.